Acta Biomaterialia 6 (2010) 856–863

Contents lists available at ScienceDirect

Acta Biomaterialia

journal homepage: www.elsevier.com/locate/actabiomat

Hydroxyapatite whisker-reinforced polyetherketoneketone bone ingrowth scaffolds

Gabriel L. Converse, Timothy L. Conrad, Christina H. Merrill, Ryan K. Roeder *

Department of Aerospace and Mechanical Engineering, University of Notre Dame, Notre Dame, IN 46556, USA

ARTICLE INFO

Article history:
Received 1 July 2008
Received in revised form 30 July 2009
Accepted 3 August 2009
Available online 6 August 2009

Keywords:
Bone ingrowth scaffolds
Composite
Hydroxyapatite
Micro-computed tomography
Polyetheretherketone

ABSTRACT

Hydroxyapatite (HA) whisker-reinforced polyetherketoneketone (PEKK) bone ingrowth scaffolds were prepared and characterized. High levels of porosity (75–90%) and HA whisker reinforcement (0–40 vol.%) were attained using a powder processing approach to mix the HA whiskers, PEKK powder and a NaCl porogen, followed by compression molding at 350–375 °C and particle leaching to remove the porogen. The scaffold architecture and microstructure exhibited characteristics known to be favorable for osteointegration. Scaffold porosity was interconnected with a mean pore size in the range 200–300 μm as measured by micro-computed tomography. HA whiskers were embedded within and exposed on the surface of scaffold struts, producing a microscale surface topography, shown by von Kossa staining and scanning electron microscopy. Therefore, HA whisker-reinforced PEKK bone ingrowth scaffolds may be advantageous for orthopedic implant fixation, including interbody spinal fusion.

1. Introduction

Orthopedic implant failure is usually due to aseptic loosening caused by several possible factors: (i) osteolysis due to wear debris, (ii) mechanical mismatch between the implant and surrounding bone tissue (stress-shielding), and (iii) relative motion between the implant and bone tissue [1]. Implant fixation has historically been achieved through the use of an acrylic cement in both orthopedics and restorative dentistry. More recently, biologic fixation has been achieved through the addition of bioactive coatings [1–5] or porosity for bone ingrowth [5–7]. Plasma-sprayed hydroxyapatite (HA) coatings promote a relatively strong tissue interface due to the bioactivity of HA, but are prone to debond from the implant surface in vivo [2–4]. Commercialized bone ingrowth scaffolds include sintered beads, wire meshes and foams composed of titanium alloys, cobalt–chrome alloys and tantalum [7]. These metallic scaffolds are generally biocompatible and osteoconductive, but are not bioactive, which may limit long-term osteointegration. Furthermore, the high X-ray attenuation of metals may inhibit post-operative radiographic analysis of bone ingrowth, which is particularly important for interbody spinal fusion [8,9].

Efforts to improve implant fixation have simultaneously investigated reductions in stiffness through implant design (e.g. cross-sectional moment of inertia) and material selection (e.g. titanium and porous metals) [6,7]. Conventional biomaterials used in most orthopedic implants today have elastic moduli at least an order of magnitude higher (e.g. cobalt–chrome, titanium and alumina) or lower (e.g. most polymers) than that of the extracellular matrix of bone tissue. Reduced implant stiffness results in increased load transfer to the peri-implant tissue, which leads to decreased bone resorption due to stress shielding and increased mechanical stimulus for new bone formation. On the other hand, the implant and biomaterials must have adequate mechanical properties to bear physiological levels of load, which is where most polymers alone, despite other advantages, fall short [10].

Polymeric scaffold materials provide unique advantages for implant fixation, including reduced stiffness compared to metallic scaffolds, radiolucency and the ability to readily incorporate bioactive fillers. Numerous polymer scaffolds have been prepared with high levels of interconnected porosity using a variety of techniques, with an emphasis placed on fabricating biodegradable scaffolds for tissue engineering applications [10–12]. Degradable polymer scaffolds have been reinforced with HA in order to improve osteointegration and mechanical properties [12–18]. Increased osteoblast proliferation and differentiation has been demonstrated on polymers reinforced with HA, compared to the unreinforced polymers [19–21]. While biodegradable polymers may be advantageous for tissue engineering scaffolds and synthetic bone graft substitutes, degradable scaffolds are not suited for improved permanent implant fixation, which remains a major clinical need.

Polyaryletherketones (PAEKs) are semicrystalline thermoplastic polymers exhibiting biochemical and biomechanical properties suitable for load-bearing orthopedic implants [8,9,22]. Dense HA-reinforced PAEK composites have been reported to exhibit mechanical properties similar to those of human cortical bone tissue [23–26]. Injection-molded polyetheretherketone (PEEK) reinforced with 10–40 vol.% HA powder was reported to exhibit an elastic modulus in the range of 4–16 GPa and tensile strength in

* Corresponding author. Tel.: +1 574 631 7003; fax: +1 574 631 2144.
E-mail address: rroeder@nd.edu (R.K. Roeder).

1742-7061/$ - see front matter © 2009 Acta Materialia Inc. Published by Elsevier Ltd. All rights reserved.
doi:10.1016/j.actbio.2009.08.004

the range of 49–83 MPa [23,24]. HA whiskers were demonstrated to result in improved tensile and fatigue properties, compared to conventional HA powders, at a given reinforcement level in polymers [27,28]. Compression-molded PEEK reinforced with 0–50 vol.% HA whiskers exhibited an elastic modulus in the range 4–23 GPa and tensile strength in the range 42–99 MPa [26]. HA whisker-reinforced PEEK also exhibited elastic anisotropy similar to that of human cortical bone, due to a preferred orientation of the HA whisker reinforcements induced during processing [26].

For the above reasons, porous HA-reinforced PAEK scaffolds may be able to improve permanent implant fixation by mitigating mechanical mismatch, promoting osteointegration and allowing radiographic analysis. However, many common methods used to prepare polymeric scaffolds are difficult or impossible with PAEK polymers due to their inherently high melting temperature (335–441 °C) and low chemical solubility [8]. HA powder-reinforced PEEK scaffolds were processed using selective laser sintering (SLS) [29–31]; however, the attainable level of porosity was limited to 70–74% which was dependent on both the reinforcement level and laser power [31]. Additionally, scaffolds became fragile as the HA content was increased, which limited the HA content to 40 wt.% or ~22 vol.% [29,30].

The objective of this study was to prepare porous HA whisker-reinforced PEKK bone ingrowth scaffolds for permanent implant fixation. Scaffolds were prepared using a combination of powder processing, compression molding and particle leaching methods. The powder processing approach was previously developed to facilitate the incorporation of high levels of HA whisker reinforcements into a polymer matrix [26–28]. Compression molding and particle leaching methods were previously used together to prepare HA-reinforced biodegradable polymer scaffolds [18,32].

2. Materials and methods

2.1. Starting powders

A commercially available PEKK powder (OXPEKK-C, Oxford Performance Materials, Enfield, CT) and sodium chloride (NaCl) powder (Product No. 71382, Fluka, Switzerland) with mean particle sizes of approximately 70 and 600 μm, respectively, were used as received. HA whiskers were synthesized using the chelate decomposition method as described in detail elsewhere [27,33]. Briefly, chemical solutions containing 0.1 M lactic acid, 0.03 M phosphoric acid and 0.05 M calcium hydroxide (all from Sigma–Aldrich, Inc., St. Louis, MO) were heated to 200 °C in 2 h and held for 2 h under static conditions in a Teflon-lined pressure vessel (Model 4600, Parr Instrument Company, Moline, IL). The as-synthesized HA whiskers were measured by optical microscopy to have a length of 21.6 (+16.9/−9.5) μm, a width of 2.8 (+0.8/−0.6) μm and an aspect ratio of 7.6 (+5.7/−3.2), where the reported values correspond to the mean (±standard deviation) of a log-normal distribution for a sample of 500 randomly selected whiskers [26].

2.2. Composite scaffold processing

Composite scaffolds with 75, 82.5 and 90% porosity were processed with 0, 20 or 40 vol.% HA whisker reinforcement. The total scaffold volume consisted of the desired pore volume plus the material volume. Thus, the reinforcement level was calculated based the desired material volume, while the porosity level was calculated based on the total scaffold volume.

Appropriate amounts of PEKK powder and HA whiskers were co-dispersed in ethanol using a sonic dismembrator (Model 500, Fisher Scientific, Pittsburgh, PA) pulsed at 1.0 cycle / s^{-1} while stirring at 1200 rpm. HA whiskers were first added to 2 ml of ethanol and ultrasonically dispersed for 1 min, followed by the addition of the PEKK powder and another 2 min of ultrasonic dispersion. After dispersion, the appropriate amount of the NaCl porogen was added to the suspension and mixed by hand using a spatula. Note that the total solids loading following the addition of the HA whiskers, PEKK powder and NaCl porogen corresponded to 50% by volume. After mixing, the viscous suspension was wet-consolidated using vacuum filtration, and the powder mixture was dried at 90 °C for at least 12 h to remove residual ethanol.

Composite scaffolds were prepared by compression molding and particle leaching. The dry powder mixture was densified at 125 MPa in a cylindrical die with a diameter of 10 mm using a manual hydraulic platen press (Model 3912, Carver Laboratory Equipment Inc., Wabash, IN). The die and densified powder mixture were then heated in a vacuum oven to the desired mold temperature and transferred back to the hydraulic platen press for compression molding at 250 MPa. Scaffolds with 82.5 and 90% porosity were molded at 350 °C, while scaffolds with 75% porosity were molded at 350, 365 and 375 °C. After cooling to room temperature, the molded composite was ejected from the die and placed in approximately 300 ml deionized water for at least 72 h to dissolve the NaCl crystals. The deionized water bath was changed daily. As-molded composite scaffolds were 10 mm in diameter and 25 mm in height.

2.3. Composite scaffold characterization

Micro-computed tomography (micro-CT) (μCT 80, Scanco Medical, Bassersdorf, Switzerland) was used to examine the porosity and architecture of the as-prepared composite scaffolds [34]. A 2 mm section from the center of each scaffold was scanned at 70 kV and 114 mA, with a voxel size of 10 μm. Two-dimensional image slices were collected, reconstructed and segmented to generate a three-dimensional binary image. Note that neat PEKK scaffolds were not able to be imaged by micro-CT due to the low X-ray attenuation of PEKK in the absence of HA reinforcement. The threshold value for segmentation was varied systematically for the level of porosity and HA content such that the porosity measured by micro-CT was not statistically different from the design porosity ($p > 0.10$, t-test).

The scaffold porosity was measured by micro-CT as:

$$P_{CT} = \left(\frac{TV - MV}{TV}\right) \cdot 100, \tag{1}$$

where TV and MV are the total volume of the scanned region and the scaffold material volume within the scanned region, respectively. Three-dimensional morphometric analysis was performed using scan data to determine the average thickness, spacing (pore size), degree of anisotropy (DA) and structure model index (SMI) of the scaffold struts. The average strut thickness and pore size were measured using the distance transformation method [35], while the degree of anisotropy was calculated using the mean intercept length method [36]. The SMI provides a non-dimensional measure of the scaffold strut morphology, where values of 0 and 3 indicate plate-like and rod-like strut morphology, respectively. The SMI was calculated as:

$$\mathrm{SMI} = \frac{6 \cdot MV}{MS^2} \cdot \frac{dMS}{dr}, \tag{2}$$

where MV and MS are the material volume and surface area, respectively, and dMS/dr is the surface area derivative [35]. The strut surface area was obtained by triangulating the strut surfaces using the marching cubes method, and the material volume was then calculated by defining polyhedra inside the triangulated surface [35,37]. The surface area derivative was estimated by a simulated

thickening of the struts and retriangulation of the strut surfaces [35]. Finally, connected component labeling was used to measure pore connectivity as the per cent of interconnected porosity voxels after thresholding [36,38].

The porosity of scaffolds processed at 375 °C with 75% design porosity were also measured by Archimedes' principle [39] in order to verify the design porosity and that measured by micro-CT. Sections of 2 mm thickness were machined from scaffolds reinforced with 20 and 40 vol.% HA whiskers using a low-speed diamond saw. The porosity of each section was first measured by micro-CT using the methods described above. Following measurement of the dry mass, the suspended and saturated mass of the sections were measured after impregnation in ethanol under vacuum for 24 h. The scaffold porosity was measured by Archimedes' principle as:

$$P_A = \frac{M - D}{M - S} \cdot \frac{100}{\rho_{Et}}, \quad (3)$$

where M, D and S are the saturated, dry and suspended masses, respectively, and ρ_{Et} is the density of ethanol.

The microstructure of selected scaffolds was also examined by scanning electron microscopy (SEM) (Evo 50, LEO Electron Microscopy Ltd., Cambridge, UK) using an accelerating voltage of 10 or 20 kV and working distance of 10–20 mm. The scaffolds were notched with a razor blade and fractured in order to reveal the internal pore structure and strut cross-sections. All specimens were coated with Au–Pd by sputter deposition.

Finally, von Kossa staining (American Mastertech Scientific) was performed on approximately 2 mm thick sections of selected scaffolds to confirm the presence of HA exposed on the surface of scaffold struts. Scaffold sections were immersed in 15 ml of 5% silver nitrate solution under UV light for 1 h, followed by 15 ml of 5% sodium thiosulfate for 3 min, and rinsed thoroughly in deionized water before and after each step. Scaffolds sections were dried in air overnight prior to optical imaging and reflected light microscopy (Eclipse ME600L, Nikon Instruments Inc., Melville, NY).

2.4. Statistical methods

Five scaffolds were prepared for each group based on porosity, HA content and mold temperature ($n = 5$). Scaffold porosity measured by micro-CT and Archimedes' principle were compared using a paired Student's t-test with a level of significance of 0.05. One-way analysis of variance (ANOVA) (StatView, SAS Institute, Inc., Cary, NC) was used to compare scaffold morphometric parameters between experimental groups. Post hoc comparisons were performed using a Tukey–Kramer HSD test with a level of significance of 0.05. Multiple ANOVA revealed that the effects of the mold temperature were not statistically significant; therefore, specimens were grouped at a similar HA content (Table 1) and two-way ANOVA was used to examine the effects of the porosity and HA content on measures of the scaffold architecture.

3. Results

3.1. Composite scaffold architecture

Three-dimensional micro-CT reconstructions enabled visualization of the porosity and architecture of HA whisker-reinforced PEKK scaffolds (Fig. 1). Two-dimensional micro-CT slices revealed uniform porosity throughout the scaffolds and confirmed that the porogen was completely removed. The mean porosity of composite scaffolds measured by micro-CT exhibited a coefficient of variation of $\leqslant$2% for any group (Table 1) and was not statistically different from measurements using Archimedes' principle. The mean (±SD) porosity of scaffolds compression molded at 375 °C with a with a design porosity of 75% and 20 vol.% HA whisker reinforcement was 75.0 ± 0.6 and 75.1 ± 0.3% when measured by micro-CT and Archimedes' principle, respectively ($p = 0.89$, paired t-test). The porosity of similar scaffolds with 40 vol.% HA whisker reinforcement was 74.5 ± 2.3 and 74.7 ± 1.0% when measured using micro-CT and Archimedes' method, respectively ($p = 0.85$, paired t-test). Greater than 99.9% of the thresholded pore volume was interconnected in all scaffolds.

Three-dimensional morphometric measurements for the scaffold architecture are listed in Table 1. Note that the effect of the mold temperature was not statistically significant for any of the measured architectural parameters; therefore, specimens were grouped at a similar HA content. The mean pore size ranged from 197 to 265 μm and, with one exception (20 vol.% HA, 82.5% porosity), was reasonably consistent between experimental groups (Table 1). The mean pore size of scaffolds with 40 vol.% HA whisker reinforcement was significantly greater than those with 20 vol.% ($p < 0.0001$, ANOVA). The pore size distribution within individual scaffolds exhibited a Gaussian distribution that consistently ranged from 10 to 600 μm. The mean strut thickness ranged from 42 to 89 μm (Table 1). The mean strut thickness increased with decreased porosity and increased HA content ($p < 0.005$, ANOVA). The scaffold architecture was nearly isotropic; the mean degree of anisotropy ranged from 1.20 to 1.26 and exhibited little interspecimen variability (Table 1). The SMI increased with increased porosity ($p < 0.0001$, ANOVA) over the range of 0.76–2.74 (Table 1).

3.2. Composite scaffold microstructure

The pore microstructure and distribution in scaffolds with 75% porosity and 20 or 40 vol.% HA whisker reinforcement molded at 365 °C appeared similar, and the polymer matrix appeared to be fully sintered (Fig. 2a and b). Scaffolds with 75% porosity and 20 or 40 vol.% HA whisker reinforcement molded at 350 and 375 °C also appeared similar to those shown in Fig. 2b. Scaffolds with 90% porosity and 0–40 vol.% HA whisker reinforcement processed at 350 °C exhibited thin struts compared to scaffolds with 75% porosity but appeared to be fully sintered (Fig. 2). However, many holes were observed in the struts of neat PEKK scaffolds at the 90%

Table 1
Porosity and morphometric parameters of HA whisker-reinforced PEKK scaffolds, showing the mean (±SD) porosity, pore size, strut thickness, degree of anisotropy (DA) and structure model index (SMI) measured by micro-CT. Differences between experimental groups not connected by the same letter were statistically significant ($p < 0.05$, Tukey–Kramer HSD test). Note that scaffolds with 75% porosity were prepared at mold temperatures of 350, 365 and 375 °C which were grouped together for 20 or 40 vol.% HA whiskers, while scaffolds with 82.5 and 90% porosity were prepared at a single mold temperature of 350 °C.

HA content (vol.%)	Design porosity (%)	Measured porosity (%)	Pore size (μm)	Strut thickness (μm)	DA	SMI
20	75.0	75.3 (0.9)	247 (26)^{a,b}	74 (8)^{a}	1.24 (0.05)^{a}	0.76 (0.22)^{a}
20	82.5	81.9 (1.0)	197 (7)^{c}	52 (3)^{b,c}	1.26 (0.02)^{a}	1.88 (0.13)^{b}
20	90.0	90.2 (1.1)	225 (12)^{b,c}	42 (1)^{c}	1.20 (0.01)^{a}	2.74 (0.10)^{c}
40	75.0	74.8 (1.5)	263 (24)^{a}	89 (13)^{d}	1.26 (0.07)^{a}	0.83 (0.16)^{a}
40	82.5	82.8 (0.3)	246 (10)^{a,b}	60 (3)^{b}	1.19 (0.01)^{a}	1.61 (0.04)^{b}
40	90.0	89.8 (0.9)	265 (14)^{a,b}	48 (2)^{b,c}	1.22 (0.01)^{a}	2.38 (0.10)^{d}

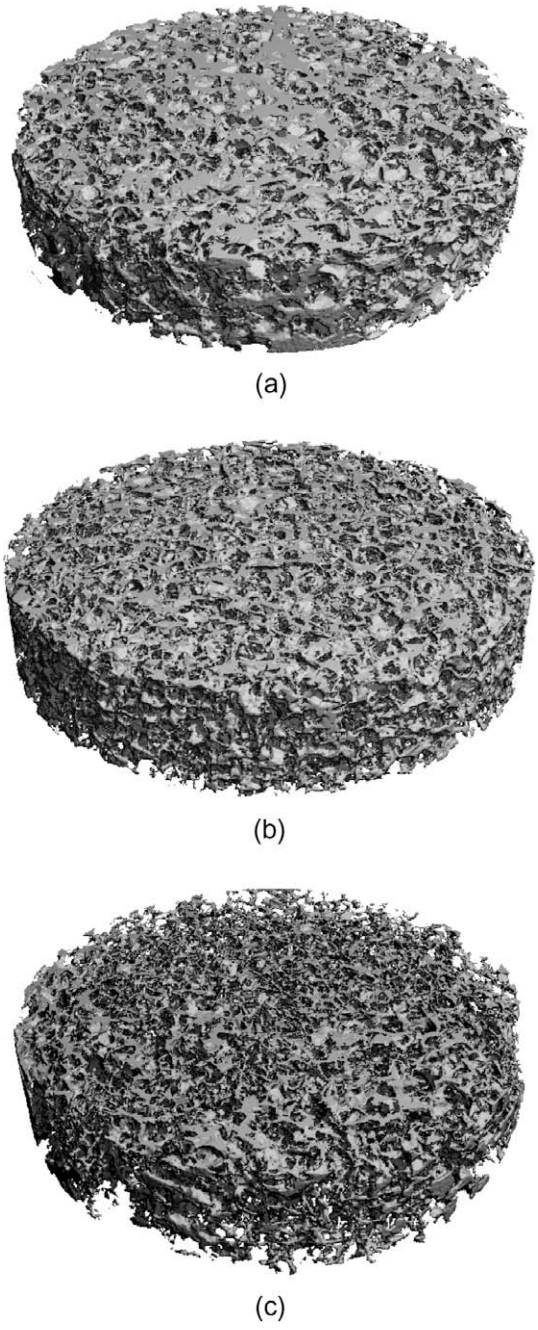

Fig. 1. Three-dimensional micro-CT reconstructions showing the porosity and architecture of 2 mm thick sections from the center of 10 mm diameter PEKK scaffolds with 40 vol.% HA whisker reinforcement and (a) 75, (b) 82.5 and (c) 90% porosity, molded at 350 °C.

porosity level compared to HA whisker-reinforced scaffolds (Fig. 2c and d). Significant variation in the strut morphology was evident within a given scaffold (Fig. 3). HA whisker reinforcements were observed to be embedded within the scaffold struts (Fig. 3c and d). HA whisker reinforcements were also observed to be exposed on the surface of scaffold struts regardless of the reinforcement content (Fig. 4), porosity level and mold temperature, resulting in a surface topography on the order of a few microns (Fig. 5). Von Kossa staining further verified that HA whiskers were exposed on the surface of scaffold struts, showing little or no staining in neat PEKK scaffolds and increased staining with increased HA content (Fig. 6).

4. Discussion

4.1. Composite scaffold processing

HA whisker-reinforced PEKK scaffolds were prepared by a combination of powder processing, compression molding and particle leaching methods. This approach circumvented the use of the organic solvents often associated with polymer scaffolds prepared using solvent casting and particle leaching methods. Polymer scaffolds processed using solvent casting techniques generally comprise a neat degradable polymer or a degradable polymer matrix reinforced with calcium phosphate particles [12]. These polymers are readily dissolved in organic solvents; however, concerns have been raised regarding the presence of residual solvent remaining after processing [12,14,32,40–42]. In contrast, PAEK polymers exhibit excellent chemical resistance, making dissolution of the polymer impractical [8]. The methods used in this study eliminated both the need to dissolve the polymer and the use of organic solvents.

The powder processing approach implemented in this study was also amenable to the addition of up to 40 vol.% HA whiskers. This is important because the extracellular matrix of human bone tissue contains 40–50 vol.% apatite crystals [43] and cellular activity on polymers has been shown to be enhanced with increased HA content [20]. If desired, even higher levels of HA whisker reinforcement may be possible because dispersion of the polymer and reinforcement phases was independent of the addition of the porogen. Previously, up to 50 vol.% HA whisker reinforcement was reliably incorporated into non-porous high-density polyethylene [27] and PEEK [26] using the same powder processing approach.

SLS was previously used to process PEEK scaffolds with 70–74% porosity and 10–40 wt.% HA powder reinforcement [29–31]. However, the scaffolds became fragile as the HA content was increased, which limited both the porosity and HA content to ~70% and 40 wt.%, respectively [29,30]. For comparison, 40 wt.% HA reinforcement in PEEK or PEKK corresponds to approximately 27 vol.%. In this study, PEKK scaffolds with 40 vol.% HA whiskers and 90% porosity were readily molded and handled after processing. Finally, the porosity of HA powder-reinforced PEEK scaffolds prepared by SLS was dependent on both the HA content and the laser power used during fabrication [31]. In contrast, the methods used in this study allowed the level of porosity to be tailored independent of the HA content by simply increasing the porogen content. Moreover, the level of porosity was tightly controlled, exhibiting low interspecimen variability (Table 1).

Possible limitations of the methods in this study include geometric constraints of compression molding and the presence of an incomplete polymer skin layer on the exterior surfaces of some as-molded scaffolds. The skin became more continuous as the mold temperature was increased. For scaffolds processed at a mold temperature of 350 °C, the skin layer did not prevent extraction of the porogen. Scaffolds processed at mold temperatures of 365 and 375 °C were lightly sanded with 600 grit SiC paper to remove the exterior skin prior to particle leaching. The composite scaffolds exhibited excellent structural integrity prior to porogen leaching, such that the sanding process did not damage the scaffolds. There was also some variation in the mean pore size between experimental groups, most notably the scaffolds with 82.5% porosity and 20 vol.% HA whiskers (Table 1). Some dissolution of salt crystals probably occurred when mixing with the PEKK powder and HA crystals in ethanol, which suggests that the time of mixing should be more highly controlled. The greater mean pore size and strut thickness of scaffolds reinforced with 40 vol.% compared to 20 vol.% HA whisker reinforcement was probably due to increased viscosity during molding at a fixed mold temperature.

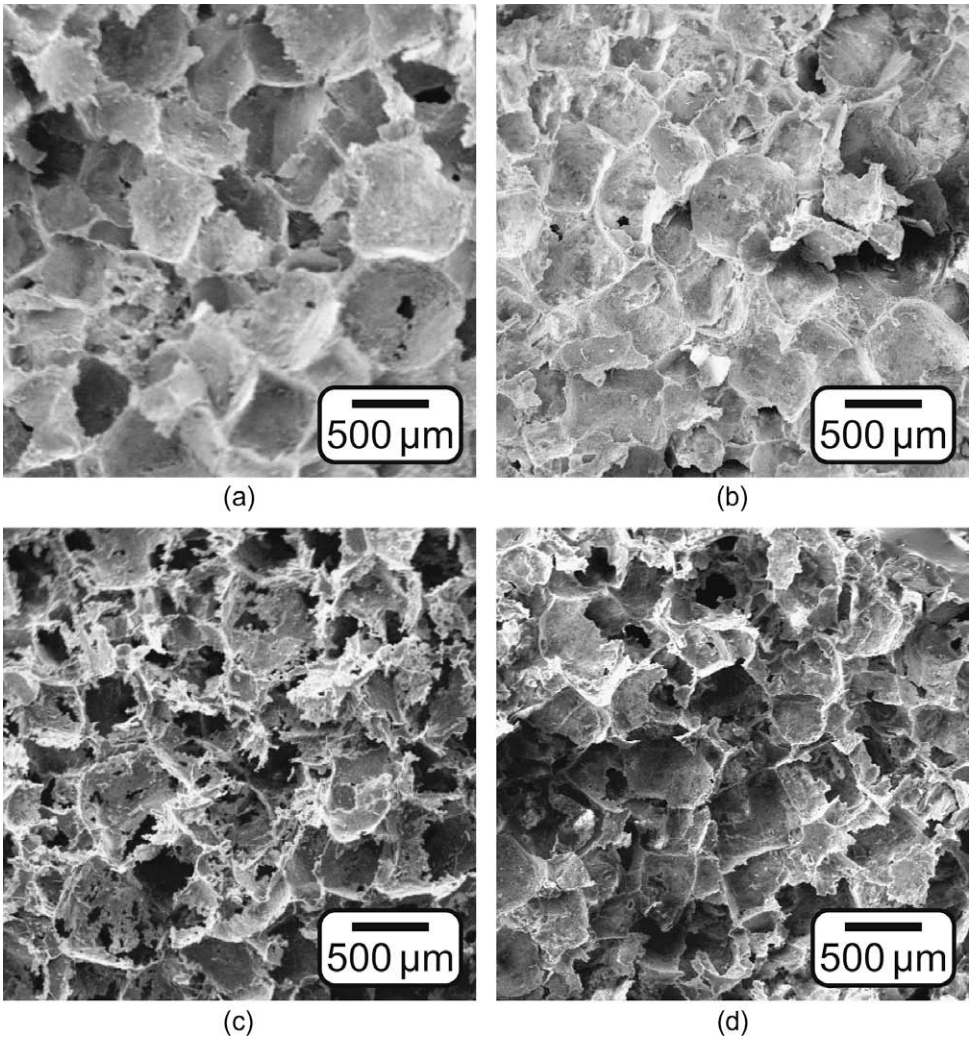

Fig. 2. SEM micrographs showing the pore structure of PEKK scaffolds with 75% porosity and (a) 20 or (b) 40 vol.% HA whisker reinforcement molded at 365 °C, and 90% porosity with (c) 0 or (d) 40 vol.% HA whisker reinforcement molded at 350 °C. Note that specimens were fractured prior to SEM observation in order to reveal the internal pore structure.

4.2. Composite scaffold architecture

Micro-CT proved useful in the characterization of HA whisker-reinforced PEKK scaffolds. Porosity and morphometric parameters were in general agreement with Archimedes' measurements and SEM observations, respectively. The accuracy of segmented micro-CT images was validated by comparing the level of porosity against paired measurements using Archimedes' principle.

Micro-CT and SEM observations indicated uniform, interconnected porosity within the composite scaffolds (Figs. 1 and 2). Bone ingrowth requires high levels of interconnected porosity with pore sizes greater than 100 μm, but optimally in the range 200–400 μm [3,4,7,44,45]. Thus, the mean pore size measured for HA whisker-reinforced PEKK scaffolds was within the "optimum" range for bone and fibrovascular tissue ingrowth (Table 1). Note that the pore size could be further tailored by sieving the porogen material prior to processing. Connected component labeling verified that greater than 99.9% of the pore volume was interconnected. The largest isolated pore volume in any scaffold was less than 50 μm in diameter if spherical.

Micro-CT measurement of the SMI and SEM observations were in close agreement, indicating a plate-like strut morphology for scaffolds with 75% porosity (Table 1; Fig. 2a and b). Interestingly, the SMI of scaffolds with 75% porosity was somewhat similar to mean values for human trabecular bone in the iliac crest (84% porosity, SMI = 1.15) and femoral head (74% porosity, SMI = 0.41) [35]. The SMI of scaffolds with 82.5 and 90% porosity indicated a more rod-like strut morphology, somewhat similar to mean values for human trabecular bone in the lumbar vertebrae (92–93% porosity, SMI = 2.12–2.13) [35], while SEM observations revealed the presence of numerous plate-like struts (Table 1, Fig. 2c and d). Discrepancy between the SMI and SEM observations for scaffolds with 82.5 and 90% porosity was most likely due to the 10 μm voxel size of the micro-CT. Strut thickness decreased with increased porosity (Table 1) and, due to variability within individual scaffolds, the thickness of some struts approached the width of individual HA whiskers (Fig. 3). As the strut thickness approached the voxel size of the micro-CT, decreased X-ray attenuation may have resulted in very thin struts being thresholded as pore space. Therefore, a small decrease in the strut surface area, *MS*, due to the erroneous inclusion of holes in plate-like struts, would be expected to result in large changes in the SMI, since the SMI depends on the square of *MS* (Eq. (2)). This explanation may at first seem contradictory to the close agreement between porosity measurements obtained

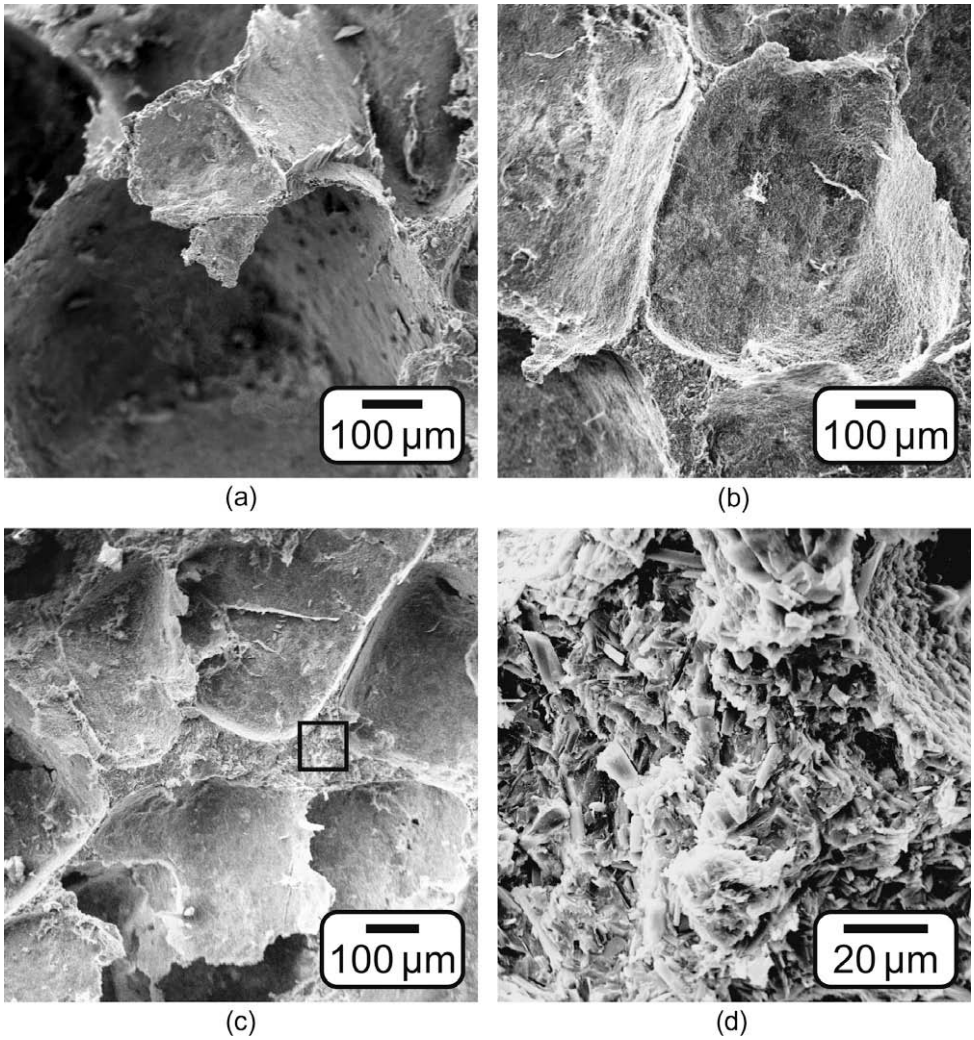

Fig. 3. SEM micrographs showing variation in strut thickness and morphology for HA whisker-reinforced PEKK scaffolds molded at 365 °C with 75% porosity and (a) 20 or (b) 40 vol.% HA whisker reinforcement. (c) SEM micrographs of a PEKK scaffold with 75% porosity and 20 vol.% HA whisker reinforcement molded at 365 °C showing (d) HA whiskers embedded within the composite struts. The area inside the box in (c) is shown at higher magnification in (d). Note that specimens were fractured prior to SEM observation in order to reveal the strut cross-sections.

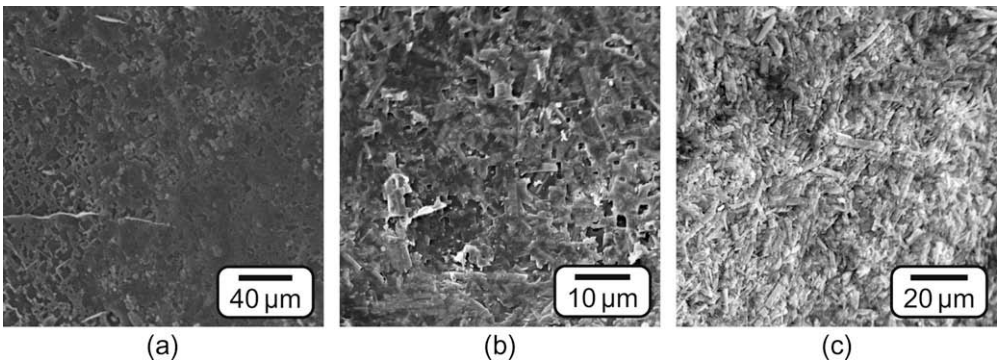

Fig. 4. SEM micrographs showing strut surfaces for PEKK scaffolds molded at 365 °C with 75% porosity and (a) 0, (b) 20 and (b) 40 vol.% HA whisker reinforcement. HA whiskers were observed to be exposed on the surface of composite struts, appearing as elongated prisms on the surface, and increased the surface roughness compared to the neat PEKK scaffold.

from micro-CT and from Archimedes' principle for scaffolds, even at 90% porosity. However, the inclusion of erroneous holes in the thinnest composite struts would be expected to result in a relatively negligible loss of material volume, *MV*, which would have little effect on the measured porosity (Eq. (1)) and SMI (Eq. (2)).

4.3. Composite scaffold microstructure

HA whiskers were observed to be exposed on the surface of composite struts (Figs. 4–6), improving the potential for cell attachment, proliferation and differentiation. HA has been shown

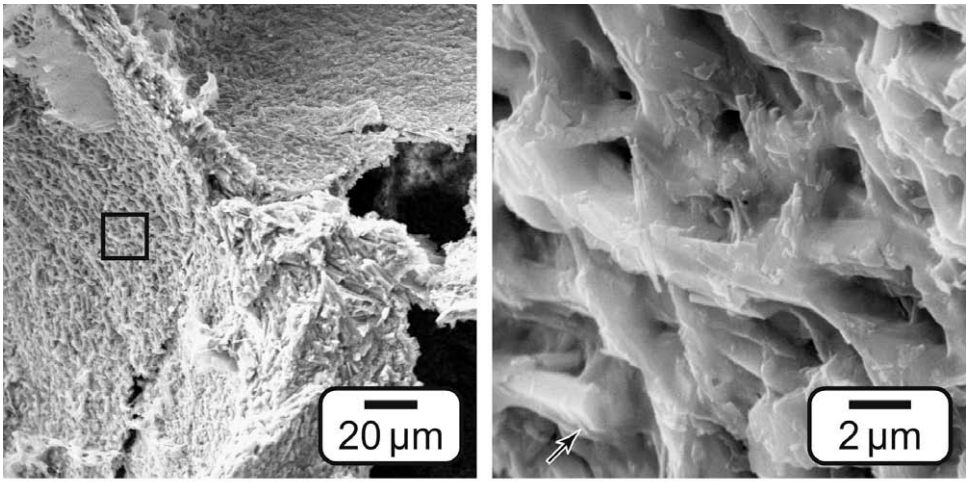

Fig. 5. SEM micrographs of a PEKK scaffold with 75% porosity and 40 vol.% HA whisker reinforcement molded at 375 °C showing the surface topology of the composite struts. The area inside the box in (a) is shown at higher magnification in (b) and the arrow highlights an HA whisker with a hexagonal prism morphology.

to be bioactive, and, if porous, to promote osteoconduction [3,4]. Increased osteoblast proliferation and differentiation has been demonstrated on polymers reinforced with HA, compared to the unreinforced polymers [19–21]. Exposed HA particles acted as preferential attachment sites for osteoblasts cultured on these composite biomaterials [19–21]. Additionally, bone morphogenetic proteins (BMPs) have been shown to adsorb onto HA through a combination of electrostatic forces and hydrogen bonding [46,47]. BMPs act as chemotactic agents, growth factors and differentiation factors, and have been used clinically to promote spinal fusion in place of an autograft [9,48,49]. Thus, the presence of exposed HA whiskers could facilitate the use and localization of BMPs within the composite scaffolds. The observed surface topology (Fig. 5) resulted from either the sintering process or the arrangement of HA whiskers within the composite struts during molding. This type of surface topology or roughness has been shown to improve cell attachment on polymer substrates [50].

HA whiskers were also observed to be embedded within the composite struts (Fig. 3c and d). Embedded whiskers acted as a reinforcement phase to improve the apparent elastic modulus and yield strength over neat PEKK scaffolds [51]. Most notably, scaffolds with 75% porosity and 20 vol.% HA molded at 375 °C exhibited a mean apparent elastic modulus and yield strength of 149 and 2.2 MPa, respectively, which was the highest of the conditions investigated and similar to human vertebral trabecular bone [51]. At all porosity and reinforcement levels, micro-CT data indicated that the composite struts were of sufficient thickness to contain embedded HA whiskers (Table 1). Micro-CT measured a mean strut thickness for a given scaffold; therefore, the standard deviations included in Table 1 do not describe the variation in strut thickness within a given scaffold. The strut thickness was observed by SEM to vary significantly within individual scaffolds (Fig. 3), presumably due to the arrangement of the salt crystals during powder processing and compression molding. Whiskers embedded within struts did not appear to be preferentially aligned (Fig. 3d), while exposed whiskers appeared somewhat aligned in a sheet texture on the surface of the strut (Fig. 4). Thus, as the thickness of a strut approached the length of the HA whiskers, the whiskers become more aligned within the plane of the strut. Finally, unreinforced scaffolds with 90% porosity exhibited an increased number of holes observed in the struts, compared to scaffolds reinforced with 40 vol.% HA whiskers at the same level of porosity (Fig. 2c and d). HA whisker reinforcement probably increased the viscosity of the polymer melt, which provided increased resistance for salt crystals coming into contact during compression molding.

5. Conclusions

HA whisker-reinforced PEKK scaffolds were prepared with 75–90% porosity and 0–40 vol.% HA whisker reinforcement. The combined powder processing, compression molding and particle leaching methods used in this study facilitated the incorporation of high levels of bioactive HA whisker reinforcements into the polymer

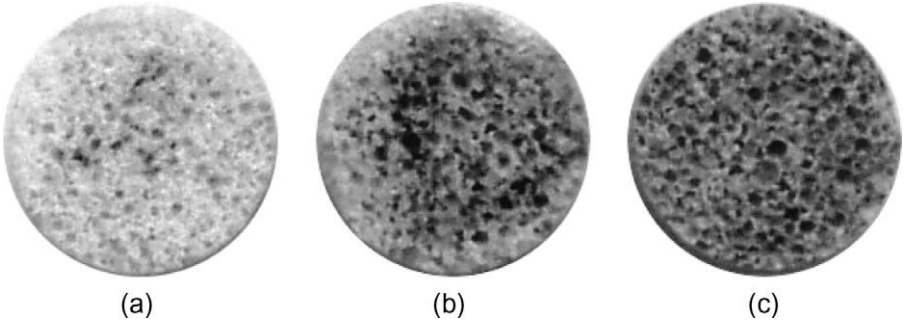

Fig. 6. Photograph of PEKK scaffolds molded at 365 °C with 75% porosity and (a) 0, (b) 20 and (b) 40 vol.% HA whisker reinforcement after von Kossa staining, showing little or no staining in the neat PEKK scaffold and increased staining (darkness) with increased HA content. Note that the scaffold diameter is 10 mm.

matrix, while avoiding the use of organic solvents. HA whiskers were both exposed on the surface and embedded within composite scaffold struts. Micro-CT indicated that the scaffold porosity was interconnected and within the size range required for bone ingrowth. Therefore, HA whisker-reinforced PEKK bone ingrowth scaffolds may be advantageous for orthopedic implant fixation, including interbody spinal fusion.

Acknowledgments

This research was partially supported by the Indiana 21st Century Research and Technology Fund and the US Army Medical Research and Materiel Command (W81XWH-06-1-0196) through the Peer Reviewed Medical Research Program (PR054672). The authors thank Glen L. Niebur and Xiutao Shi at Notre Dame for assistance with micro-computed tomography measures for the scaffold architecture.

References

[1] Vander Sloten J, Labey L, Van Audekercke R, Van der Perre G. Materials selection and design for orthopaedic implants with improved long-term performance. Biomaterials 1998;19(16):1455–9.
[2] Cheang P, Khor KA. Addressing processing problems associated with plasma spraying of hydroxyapatite coatings. Biomaterials 1996;17(5):534–7.
[3] Hench LL. Bioceramics: from concept to clinic. J Am Ceram Soc 1991;74(7):1487–510.
[4] LeGeros RZ. Properties of osteoconductive biomaterials: calcium phosphates. Clin Orthop Relat Res 2002;(395):81–98.
[5] Sporer SM, Paprosky WG. Biologic fixation and bone ingrowth. Orthop Clin North Am 2005;36(1):105–11.
[6] Bobyn JD, Mortimer ES, Glassman AH, Engh CA, Miller JE, Brooks CE. Producing and avoiding stress shielding. Laboratory and clinical observations of noncemented total hip arthroplasty. Clin Orthop Related Res 1992;(274):79–96.
[7] Ryan G, Pandit A, Apatsidis DP. Fabrication methods of porous metals for use in orthopaedic applications. Biomaterials 2006;27(13):2651–70.
[8] Kurtz SM, Devine JN. PEEK biomaterials in trauma, orthopedic, and spinal implants. Biomaterials 2007;28:4845–69.
[9] Toth JM, Wang M, Estes BT, Scifert JL, Seim 3rd HB, Turner AS. Polyetheretherketone as a biomaterial for spinal applications. Biomaterials 2006;27:324–34.
[10] Rose FRAJ, Oreffo ROC. Bone tissue engineering: hope vs hype. Biochem Biophys Res Comm 2002;292:1–7.
[11] Agrawal CM, Ray RB. Biodegradable polymeric scaffolds for musculoskeletal tissue engineering. J Biomed Mater Res 2001;55(2):141–50.
[12] Rezwan K, Chen QZ, Blaker JJ, Boccaccini AR. Biodegradable and bioactive porous polymer/inorganic composite scaffolds for bone tissue engineering. Biomaterials 2006;27:3413–31.
[13] Causa F, Netti PA, Ambrosio L, Ciapetti G, Baldini N, Pagani S, et al. Poly-epsilon-caprolactone/hydroxyapatite composites for bone regeneration: In vitro characterization and human osteoblast response. J Biomed Mater Res 2006;76A:151–62.
[14] Kim SS, Sun Park M, Jeon O, Yong Choi C, Kim BS. Poly(lactide-co-glycolide)/hydroxyapatite composite scaffolds for bone tissue engineering. Biomaterials 2006;27(8):1399–409.
[15] Kothapalli CR, Shaw MT, Wei M. Biodegradable HA-PLA 3-D porous scaffolds: effect of nano-sized filler content on scaffold properties. Acta Biomater 2005;1:653–62.
[16] Mathieu LM, Mueller TL, Bourban PE, Pioletti DP, Muller R, Manson JA. Architecture and properties of anisotropic polymer composite scaffolds for bone tissue engineering. Biomaterials 2006;27:905–16.
[17] Shor L, Guceri S, Wen X, Gandhi M, Sun W. Fabrication of three-dimensional polycaprolactone/hydroxyapatite tissue scaffolds and osteoblast-scaffold interactions in vitro. Biomaterials 2007;28:5291–7.
[18] Thomson RC, Yaszemski MJ, Powers JM, Mikos AG. Hydroxyapatite fiber reinforced poly(α-hydroxy ester) foams for bone regeneration. Biomaterials 1998;19:1935–43.
[19] Dalby MJ, Di Silvio L, Harper EJ, Bonfield W. In vitro evaluation of a new polymethylmethacrylate cement reinforced with hydroxyapatite. J Mater Sci Mater Med 1999;10:793–6.
[20] Di Silvio L, Dalby MJ, Bonfield W. Osteoblast behaviour on HA/PE composite surfaces with different HA volumes. Biomaterials 2002;23(1):101–7.
[21] Zhang Y, Tanner KE, Gurav N, Di Silvio L. In vitro osteoblastic response to 30 vol.% hydroxyapatite-polyethylene composite. J Biomed Mater Res 2007;81A:409–17.
[22] Evans SL, Gregson PJ. Composite technology in load-bearing orthopaedic implants. Biomaterials 1998;19(15):1329–42.
[23] Abu Bakar MS, Cheang P, Khor KA. Mechanical properties of injection molded hydroxyapatite–polyetheretherketone biocomposites. Comp Sci Technol 2003;63:421–5.
[24] Abu Bakar MS, Cheng MH, Tang SM, Yu SC, Liao K, Tan CT, et al. Tensile properties, tension-tension fatigue and biological response of polyetheretherketone-hydroxyapatite composites for load-bearing orthopedic implants. Biomaterials 2003;24(13):2245–50.
[25] Tang SM, Cheang P, Abu Bakar MS, Khor KA, Liao K. Tension-tension fatigue behavior of hydroxyapatite reinforced polyetheretherketone composites. Int J Fatigue 2004;26:49–57.
[26] Converse GL, Yue W, Roeder RK. Processing and tensile properties of hydroxyapatite-whisker-reinforced polyetheretherketone. Biomaterials 2007;28(6):927–35.
[27] Roeder RK, Sproul MM, Turner CH. Hydroxyapatite whiskers provide improved mechanical properties in reinforced polymer composites. J Biomed Mater Res 2003;67A(3):801–12.
[28] Kane RJ, Converse GL, Roeder RK. Effects of the reinforcement morphology on the fatigue properties of hydroxyapatite reinforced polymers. J Mech Behav Biomed Mater 2008;1(3):261–8.
[29] Tan KH, Chua CK, Leong KF, Cheah CM, Cheang P, Abu Bakar MS, et al. Scaffold development using selective laser sintering of polyetheretherketone-hydroxyapatite biocomposite blends. Biomaterials 2003;24:3115–23.
[30] Tan KH, Chua CK, Leong KF, Cheah CM, Gui WS, Tan WS, et al. Selective laser sintering of biocompatible polymers for applications in tissue engineering. Biomed Mater Eng 2005;15:113–24.
[31] Tan KH, Chua CK, Leong KF, Naing MW, Cheah CM. Fabrication and characterization of three-dimensional poly(ether-ether-ketone)/-hydroxyapatite biocomposite scaffolds using laser sintering. Proc Inst Mech Eng: Part H, J Eng Med 2005;219:183–94.
[32] Jung Y, Kim SS, Kim YH, Kim SH, Kim BS, Kim S, et al. A poly(lactic acid)/calcium metaphosphate composite for bone tissue engineering. Biomaterials 2005;26:6314–22.
[33] Roeder RK, Converse GL, Leng H, Yue W. Kinetic effects on hydroxyapatite whiskers synthesized by the chelate decomposition method. J Am Ceram Soc 2006;89(7):2096–104.
[34] ASTM Standard F2450-04. Standard Guide for Assessing Microstructure of Polymeric Scaffolds for Use in Tissue Engineered Medical Products. West Conshohocken, PA: American Society for Testing and Materials; 2004.
[35] Hildebrand T, Laib A, Muller R, Dequeker J, Ruegsegger P. Direct three-dimensional morphometric analysis of human cancellous bone: microstructural data from spine, femur, iliac crest, and calcaneus. J Bone Miner Res 1999;14:1167–74.
[36] Odgaard A. Three-dimensional methods for quantification of cancellous bone architecture. Bone 1997;20(4):315–28.
[37] Hildebrand T, Ruegsegger P. Quantification of bone microarchitecture with the structure model index. Comput Methods Biomech Biomed Eng 1997;1:15–23.
[38] H. Samet. Applications of spatial data structures. Reading, MA: Addison-Wesley; 1990. p. 185–223.
[39] ASTM Standard C373-88. Standard test method for water absorption, bulk density, apparent density and the apparent specific gravity of fired whiteware products. West Conshohocken, PA: American Society of Testing Materials; 1999.
[40] Harris LD, Kim BS, Mooney DJ. Open pore biodegradable matrices formed with gas foaming. J Biomed Mater Res 1998;42:396–402.
[41] Lee SH, Kim BS, Kim SH, Kang SW, Kim YH. Thermally produced biodegradable scaffolds for cartilage tissue engineering. Macromol Biosci 2004;4:802–10.
[42] Mooney DJ, Baldwin DF, Suh NP, Vacanti JP, Langer R. Novel approach to fabricate porous sponges of poly(D,L-lactic-co-glycolic acid) without the use of organic solvents. Biomaterials 1996;17:1417–22.
[43] Rho J-Y, Kuhn-Spearing L, Zioupos P. Mechanical properties and the hierarchical structure of bone. Med Eng Phys 1998;20:92–102.
[44] Boyan BD, Hummert TW, Dean DD, Schwartz Z. Role of material surfaces in regulating bone and cartilage cell response. Biomaterials 1996;17:137–46.
[45] Karageorgiou V, Kaplan D. Porosity of 3-D biomaterial scaffolds and osteogenesis. Biomaterials 2005;26:5474–91.
[46] Dong X, Wang Q, Wu T, Pan H. Understanding adsorption-desorption dynamics of BMP-2 on hydroxyapatite (0 0 1) surface. Biophys J 2007;93:750–9.
[47] Zhou H, Wu T, Dong X, Wang Q, Shen J. Adsorption mechanism of BMP-7 on hydroxyapatite (0 0 1) surfaces. Biochem Biophys Res Commun 2007;361:91–6.
[48] Subach BR, Haid RW, Rodts GE, Kaiser MG. Bone morphogenetic protein in spinal fusion: overview and clinical update. Neurosurg Focus 2001;10:E3.
[49] Mummaneni PV, Pan J, Haid RW, Rodts GE. Contribution of recombinant human bone morphogenetic protein-2 to the rapid creation of interbody fusion when used in transforaminal lumbar interbody fusion: a preliminary report. Invited submission from the joint section meeting on disorders of the spine and peripheral nerves. J Neurosurg Spine 2004;1:19–23.
[50] Lampin M, Warocquier-Clerout, Legris C, Degrange M, Sigot-Luizard MF. Correlation between substratum roughness and wettability, cell adhesion, and cell migration. J Biomed Mater Res 1997;36:99–108.
[51] Converse GL, Conrad TL, Roeder RK. Mechanical properties of hydroxyapatite whisker reinforced polyetherketoneketone composite scaffolds. J Mech Behav Biomed Mater; in press.